2022

Double-Lift Ammonia/Water Compression-Resorption Heat Pump for Simultaneous Industrial Process Heating and Refrigeration Applications

Dereje Sendeku Ayou

Alberto Coronas

Double-Lift Ammonia/Water Compression-Resorption Heat Pump for Simultaneous Industrial Process Heating and Refrigeration Applications

Dereje S. AYOU* and Alberto CORONAS

Universitat Rovira i Virgili, Department of Mechanical Engineering, CREVER-Group of Applied Thermal Engineering, Av. Països Catalans 26, 43007 Tarragona, Spain

* Corresponding Author: E-mail: derejesendeku.ayou@urv.cat, Phone: +34 977 55 96 65

ABSTRACT

The hybridization of absorption and compression heat pump cycles is a promising way to increase the temperature lift and heat sink temperature of industrial heat pumps with acceptable performance. This paper presents a novel double-lift ammonia/water compression-resorption heat pump (DL-CRHP) cycle for the process heating and refrigeration applications in the food and beverages processing industry. The DL-CRHP allows the integration of industrial refrigeration operation, as a heat source, into process heat production at high temperature using a single heat pump with a reduced capital cost and minimal loss of exergy than the separate provision of process heating and refrigeration. The DL-CRHP cycle consists of an evaporator-condenser loop for refrigeration <15 °C and a resorption cycle solution loop, which comprises an absorber and a desorber, for process heat supply at high-temperature level (≥100 °C). The dry R717 vapor compression is carried out in two stages due to the required large-temperature-lift of simultaneous process heating and refrigeration applications in the food and beverages industry, and technical constraints of market-available R717 compressor technologies. The DL-CRHP performance is improved by using refrigerant and solution internal heat recuperators. The present study aims to evaluate the performance of this heat pump cycle by using a simulation model developed under steady-state conditions. At the heat pump cycle design condition, the refrigeration capacity of the evaporator is set to 500 kW with a chilled fluid (ethylene glycol/water mixture) supply temperature between −10 °C and 10 °C, and the temperature glides in the heat sink (hot water) and source (chilled fluid) are 30 K and 10 K, respectively. The effect of hot water and chilled fluid supply temperatures on the heat pump's energetic and exergetic performances was investigated to identify the working domain of the proposed heat pump under imposed component's technical constraints. Simulation results show that the combined heating and refrigeration COP of about 2.02–4.04 and exergy efficiency of 0.467– 0.483 was attainable with a heat sink outlet temperature of 100–150 °C and refrigeration effect at a temperature between −10 °C and 10 °C. The use of a vapor-liquid (internal) heat exchanger allows for reducing the high-pressure compression stage discharge temperature below the current limit of R717 compressor technologies (≤190 °C) in most operating conditions. The development of this type of heat pump, characterized by large-temperature-lift and high heat sink temperature, plays a significant role in the decarbonization of the food and beverage industry, and other industrial applications need simultaneous heating and refrigeration.

Keywords: ammonia/water, compression-resorption, double-lift, heat pump, process heating, industrial refrigeration

1. INTRODUCTION

The global population is growing and is expected to rise by 2 billion persons in the next 30 years reaching 9.7 billion in 2050 according to the United Nations projection. Food demands are also estimated to rise by 60% in 2050 (Ladha-Sabur *et al.*, 2019). Moreover, the food and beverage sector is heavily dependent on fossil fuels and considerably contributes to the global greenhouse (GHG) emissions. Hence, the food and beverage processing industries should regularly be aware of their energy consumption (i.e., fuel and electricity), as the current and new regulations at the national/international levels and legal requirements demand a reduction of energy consumption and GHG emissions to combat climate change. For instance, the estimated thermal energy and electrical energy needed per metric ton of produced product across the leading European countries in this sector (i.e., Austria, France, Germany, Poland, Spain, and the UK) are about 1055 (129–3957) kWh/ton of thermal and 625 (21–3636) kWh/ton of electrical energies for the dairy while 317 (56–1950) kWh/ton of thermal and 253 (14–800) kWh/ton of electrical energies for the beverages industry (Meyers *et al.*, 2016). Thus, energy efficiency enhancement and the use of renewable sources using efficient heating and refrigeration technologies like heat pumps have been recognized as key pathways for the abatement of energy consumption related GHG emissions.

A heat pump has the unique ability to deliver both heating and refrigeration, simultaneously, which allows very high primary energy conversion efficiencies and low emission of CO_2 per unit of supplied useful output (heating or refrigeration) especially if non-renewable driving energy sources are utilized. The deployment of these types of heat pumps shows great promise for industries that need significant process heating and refrigeration simultaneously or within a short duration, which is often found in the food and beverage sector. An R717 vapor compressor heat pump using a screw compressor technology was integrated into a chocolate factor in the UK, where the glycol loop was chilled from 5 °C to 0 °C at a refrigeration rate of 914 kW while process water was heated from 10 °C to 60 °C at a heating rate of 1250 kW yielding at combined COP of around 6.25 (IEA, 2014). A single-stage ammonia/water absorption heat pump was developed and field demonstrated in a poultry processing plant in California (the United States) to supply heating at 60 °C and a chilling effect between −9 °C to 5 °C using driving heat at 135 °C provided by a natural gas-fired hot water boiler (Erickson *et al.*, 2014). This heat pump can deliver heat up to 90 °C, and co-producing refrigeration, by increasing the temperature of the driving heat. However, there are several unit processes like drying, evaporation, sterilization, etc. require heating at high-temperature levels (>100 °C) in the food and beverage industries while refrigeration (<15 °C) is required for process cooling and product storage applications. Traditionally, these heating and refrigeration demands are supplied using fossil-fuel-fired boilers and electricity-driven refrigeration systems (Liu *et al.*, 2017).

This paper aims to investigate (i) the operational map and (ii) evaluate the first-law and second-law efficiencies of a novel double-lift ammonia/water compression-resorption heat pump (DL-CRHP) for providing hot water in the range of 100–150 °C while producing refrigeration between –10 °C and 10 °C, which is suitable for process heating and refrigeration applications in the food and beverages industry. The paper is structured as follows: first, the proposed heat pump cycle is described (Section 2), and details of the steady-state modelling of the DL-CRHP are presented in Section 3; then, Section 4 presents and discusses the obtained simulation results and, finally, the paper concludes with a summary of the key findings in Section 5.

2. HEAT PUMP CYCLE DESCRIPTION

Figure 1 depicts the schematic of the novel DL-CRHP cycle for simultaneous process heating and refrigeration applications. This high-temperature heat pump (HTHP) cycle can deliver heat at a temperature above 100 °C while operating at a large-temperature-lift to provide refrigeration below 0 °C by using market-available (standard) components of R717 heat pumps.

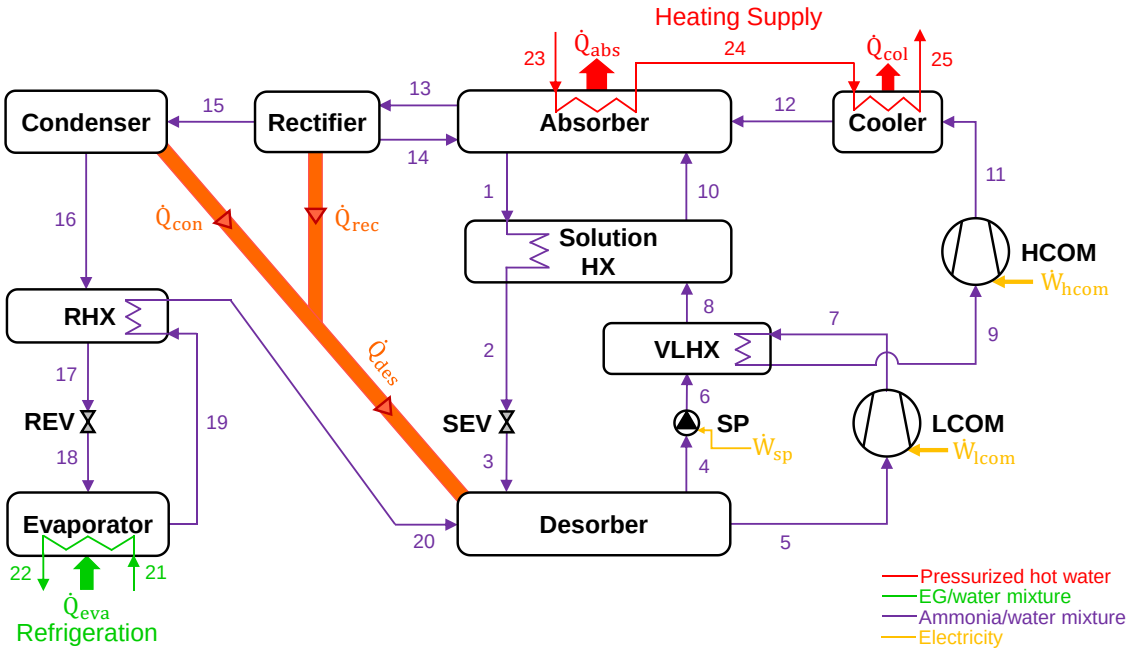

Figure 1: Schematic of the double-lift two-stage ammonia/water compression-resorption heat pump (DL-CRHP) cycle for simultaneous industrial process heating and refrigeration applications

The DL-CRHP cycle is designed to supply heating (stream 23→24→25) and refrigeration (stream 21→22) demands of the food and beverage processing industries. In this double-lift heat pump, the reversed solution loop of the resorption cycle comprises an absorber (also referred to as a resorber), a desorber, a solution heat exchanger (SHX), a solution pump (SP), and a solution expansion valve (SEV) as shown in Figure 1. The cycle has two dry-compression stages (low-pressure stage, LCOM, and high-pressure stage, HCOM) connected in series due to the required large-temperature-lift for the chosen simultaneous process heating and refrigeration applications. The vapor-liquid (internal) heat exchanger (VLHX) is used for intercooling the compressor's discharge vapor between the two compression stages (i.e., LCOM and HCOM). The heat rejected during ammonia/water vapor rectification (stream 13→14 and 15) and condensation (stream 15→16) processes are utilized for the desorption of the strong (in ammonia) ammonia/water solution (stream 1→2→3) in the desorber. The resorption solution loop (circuit) lifts the condenser temperature to a high temperature, which it can be delivered as useful heat using a closed pressurized hot water loop (stream 23→24). Additionally, the heat released during the desuperheating of the HCOM discharge vapor (stream 11→12) in the gas cooler, before entering the absorber, is used to raise the temperature of the heat sink fluid leaving the absorber (stream 24→25). Thereby, the resorption sub-cycle (resorption loop) delivers high-temperature useful heat (stream 23→25; $t_{25} \geq$100 °C) with wide design flexibility on the temperature glide of secondary fluid of the heat sink. The refrigeration sub-cycle (stream 13→15{and 14}→16→17→18→19→20) comprises a condenser, an evaporator, a rectifier, a refrigerant expansion valve (REV), and a refrigerant heat exchanger (RHX), and it supplies the refrigeration output of the DL-CRHP cycle as illustrated in Figure 1. The weak ammonia/water solution (stream 4→6→8→10) is preheated, before entering the absorber, in the VLHX (stream 6→8) and SHX (stream 8→10) using the vapor discharged from the LCOM (stream 7→9) and strong solution from the absorber (stream 1→2).

The use of the DL-CRHP cycle using ammonia/water mixture as working fluid, instead of a two-stage R717 heat pump, has several benefits including the operation of the heat pump at lower system high-pressure while reaching a higher heat sink temperature. Furthermore, the resorption sub-cycle of the DL-CRHP can be designed to fit well the required heat source and sink temperature glides since it has temperature gliding in the heat addition (desorption) and heat rejection (absorption) processes adjusted by the composition of ammonia/water mixture and mass flow rate of the ammonia/water solutions (i.e., solution circulation ratio).

3. MODELING METHODOLOGY

To evaluate the performance of the proposed DL-CRHP, a system model has been developed and the model equations are solved using the Engineering Equation Solver (EES) platform. This simulation model is based on models of each system component. Some reasonable and common assumptions are adopted (Herold *et al.*, 2016; Jensen *et al.*, 2015):

- The heat pump cycle is operating under steady-state conditions since steady-state performance under different working conditions, instead of transient performance, is focused on the characterization of the DL-CRHP.
- Heat losses and pressure drops are neglected in heat and/or mass exchangers and connecting pipelines.
- The liquid solution and vapor leaving the desorber are saturated at the corresponding pressure and temperature.
- The vapor leaving the absorber (stream 13) is saturated at the corresponding temperature and pressure. The saturated ammonia/water solution in equilibrium with this vapor (stream 13) is mixed with the liquid condensate leaving the rectifier (stream 14) before entering the SHX (stream 1).
- The liquid refrigerant leaving the condenser (stream 16) is saturated. Partial vaporization is allowed at the exit of the evaporator (stream 19) at its operating pressure (system low pressure).
- All expansion valves (i.e., REV and SEV) are operating adiabatically (isenthalpic process).

The steady-state models of each component (unit, u) of the DL-CRHP are based on mass and energy conservation equations and imposed constraints according to the second law of thermodynamics in all components. The mass and energy balances of each component are expressed by generic Equations (1) – (3) considering the above assumptions.

Overall mass balance for unit (u)

$$\sum_{i \in IN(u)} \dot{m}_i - \sum_{i \in OUT(u)} \dot{m}_i = 0 \quad (1)$$

where $\dot{m}_i$ is the mass flow rate of stream i, $IN(u)$ designates the inflowing streams into unit u, and $OUT(u)$ indicates the set of outgoing streams from the unit u.

Component (ammonia) mass balance:

$$\sum_{i \in IN(u)} z_i \, \dot{m}_i - \sum_{i \in OUT(u)} z_i \, \dot{m}_i \; = \; 0 \tag{2}$$

where z_i is the ammonia mass fraction of stream *i*.

Energy balance for unit (*u*):

$$\sum_{i \in IN(u)} h_i \, \dot{m}_i \; - \sum_{i \in OUT(u)} h_i \, \dot{m}_i \; + \; \dot{W}_u \; - \; \dot{Q}_u \; = \; 0 \tag{3}$$

where h_i is the specific enthalpy of stream *i*, and $\dot{Q}_u$ and $\dot{W}_u$ are the heat flow and work flow rates, respectively, into or out of the control volume for unit *u*.

The DL-CRHP cycle operates at three pressure levels, which are high pressure (P_{high}), low pressure (P_{low}), and intermediate pressure (P_{mid}) was determined by the geometric mean pressure ($P_{mid} = \sqrt{P_{low} P_{high}}$) without optimization, ensuring an equal pressure ratio (pr_{com}) in both LCOM and HCOM. Also, it should be noted that there is an optimum intermediate pressure that maximize the performance of a heat pump using a two-stage compressor, which may be expressed as $P_{mid} = \beta \sqrt{P_{low} P_{high}}$, where $\beta > 1.0$. The LCOM and HCOM of the heat pump are modeled as piston compressors since real installations of ammonia/water compression-resorption heat pumps are using piston compressor technology (Wersland *et al.*, 2017). To determine the exhaust (discharge) conditions after the compression process, the isentropic efficiency of the compressor ($\eta_{ise,com}$) is defined as:

$$\eta_{ise,com} = \frac{h_{com,ex,ise} - h_{com,su}}{h_{com,ex} - \; h_{com,su}} \tag{4}$$

where $h_{com,su}$ and $h_{com,ex}$ are the compressor suction and exhaust working fluid vapor enthalpies in kJ kg^{-1}, and $h_{com,ex,ise}$ is the ideal exhaust working fluid vapor enthalpy with an isentropic compression process in kJ kg^{-1}. The $\eta_{ise,com}$ is calculated for piston compressor using Equation 5, which is mainly dependent on pr_{com} in case of piston compressor (Wersland *et al.*, 2018). Also, Jørgensen *et al.* (2021) used an average isentropic efficiency value of 0.79 and 0.83 for the low-stage compressor (<28 bar discharge pressure) and high-stage compressor (<50/60 bar discharge pressure), respectively, by investigating isentropic efficiencies of piston compressors from several suppliers.

$$\eta_{ise,com} = 0.7876 - 0.0006 pr_{com} \tag{5}$$

The electrical power consumption of compressor, $\dot{W}_{com,el}$ in kW, is calculated using Equation 6.

$$\dot{W}_{com,el} = \frac{\dot{m}_{com} \left(h_{com,ex} - h_{com,su} \right)}{\eta_m} \tag{6}$$

where $\dot{m}_{com}$ is vapor mass flow rate (kg/s) through the compressor and η_m is electric motor efficiency (95%).

The volumetric efficiency of piston compressor, λ_{com}, is calculated as (Wersland et al., 2018, 2017):

$$\lambda_{com} = \eta_{vol,com} \, \eta_d = 1.0056 \; - \; 0.0374 pr_{com} \tag{7}$$

where $\eta_{vol,com}$ is clearance volume efficiency (-) and η_d is the loss factor (-). The stroke volumes of the compressors are obtained using Equation 8.

$$V_S = \frac{\dot{m}_{com} v_{com,su}}{\lambda_{com} n} \tag{8}$$

where $v_{com,su}$ is suction line specific volume in m^3 kg^{-1} and *n* is the frequency in *Hz*.

Besides, the compressor was modeled by considering a heat loss factor of 10% for its power consumption, which is typical for large-scale piston compressors (Jørgensen *et al.*, 2021; Ommen *et al.*, 2019).

The solution pump electrical power consumption, $\dot{W}_{sp,el}$ in kW, is calculated using Equation 9.

$$\dot{W}_{sp,el} = \frac{\dot{m}_{com} v_{com,su} \left(P_{high} - P_{low}\right)}{\eta_{sp} \eta_m} \tag{9}$$

where η_{sp} and η_m are the pump efficiency (75%) and electric motor efficiency driving the pump (95%).

The heat duty, $\dot{Q}_u$ in kW, of the heat and/or mass exchangers is calculated by the heat transfer equation:

$$\dot{Q}_u = (UA)_u \Delta T_{lmtd,u} \tag{10}$$

where UA is overall heat transfer conductance (product of overall heat transfer coefficient, U in kW m^{-2} K^{-1}, and surface area, A in m^2) and ΔT_{lmtd} is the logarithmic mean temperature difference (in K). The internal heat recuperators (i.e., SHX and RHX) and HCOM vapor exhaust desuperheater (cooler) are modeled by using the heat exchanger effectiveness model, Equation 11, with a fixed effectiveness value (Jensen et al., 2015). The required size of the VLHX is determined by imposing a degree of superheat of 1 K at the suction of the HCOM.

$$\dot{Q}_u = \varepsilon_u \dot{C}_{min} \left(t_{h,in} - t_{c,in}\right) \tag{11}$$

where ε_u is effectiveness of the heat exchanger (-), $\dot{C}_{min}$ is the minimum heat capacity rate (kW °C^{-1}), $t_{h,in}$ and $t_{c,in}$ are the hot fluid and cold fluid stream inlet temperatures.

The heat released during the rectification and (then) condensation of the ammonia/water vapor from the absorber (stream 13→15{and 14} →16) is used in the desorption process of the strong solution from the absorber after heat recovery in the SHX as depicted in Figure 2. The liquid stream leaving the rectifier (stream 14) is in equilibrium with the vapor entering it (stream 13) for an ideal rectifier (i.e., $t_{14} = t_{13}$) (Herold *et al.*, 2016). Since heat loss from the components including the separator, except the compressors, was neglected a thermodynamic equilibrium between the vapor and liquid phases was assumed. Thereby, the temperatures of streams leaving the separator are the same (i.e., $t_4 = t_5$). The temperature at the exit of the condenser (t_{16}) is set equal to the desorber exit temperature (t_{27}) for the internal heat exchange between the condenser, desorber, and rectifier (i.e., $t_{16} = t_{27}$).

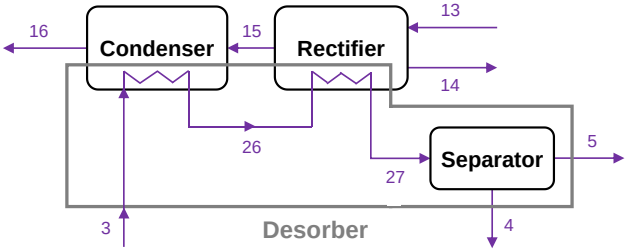

Figure 2: Schematic of an integrated condenser-desorber-rectifier unit of the proposed ammonia/water DL-CRHP.

The DL-CRHP performance is evaluated based on the first-law and second-law of thermodynamics. The combined *COP* for the simultaneous heating and refrigerating supply, COP_{shr}, is defined as:

$$COP_{shr} = \frac{\dot{Q}_{abs} + \dot{Q}_{col} + \dot{Q}_{eva}}{\dot{W}_{lcom,el} + \dot{W}_{hcom,el} + \dot{W}_{sp,el}} \tag{12}$$

where $\dot{Q}_{abs}$ is the absorber heat duty in kW, $\dot{Q}_{col}$ is the gas cooler heat duty in kW, and $\dot{Q}_{eva}$ is evaporator heat duty (i.e., refrigeration capacity of the heat pump) in kW. The heating capacity of the heat pump is the sum of the absorber and cooler heat duties ($\dot{Q}_h = \dot{Q}_{abs} + \dot{Q}_{col}$). $\dot{W}_{lcom,el}$ and $\dot{W}_{hcom,el}$ are power consumption of the LCOM and HCOM.

The second-law efficiency of the DL-CRHP, $\eta_{II,shr}$, is defined as:

$$\eta_{II,shr} = \frac{COP_{shr}}{COP_{ideal,shr}} = \left(\frac{\bar{T}_{hw} - \bar{T}_{cf}}{\bar{T}_{hw} + \bar{T}_{cf}}\right) COP_{shr} \tag{13}$$

where $COP_{ideal,shr}$ is the combined *COP* of reversible DL-CRHP cycle operates at two-temperature levels. $\bar{T}_{cf}$ and $\bar{T}_{hw}$ are the entropic average temperatures for chilled fluid stream (30% EG/water mixture) and the heating supply stream (pressurized hot water), respectively.

The exergy efficiency of the DL-CRHP, $ECOP_{shr}$, can be expressed as follows:

$$ECOP_{shr} = \frac{\left(\dot{Q}_{abs} + \dot{Q}_{col}\right)\left(1 - \frac{T_0}{\bar{T}_{hw}}\right) + \dot{Q}_{eva}\left(1 - \frac{T_0}{\bar{T}_{cf}}\right)}{\dot{W}_{lcom,el} + \dot{W}_{hcom,el} + \dot{W}_{sp,el}} \tag{14}$$

where T_0 is the dead state temperature taken as 288 K (15°C).

The volumetric capacity for simultaneous heating and refrigeration delivery, *VSHR* in kJ/m^3, is computed as:

$$VSHR = \frac{\dot{Q}_{abs} + \dot{Q}_{col} + \dot{Q}_{eva}}{\dot{V}_{lcom} + \dot{V}_{hcom}} \tag{15}$$

where $\dot{V}_{lcom}$ and $\dot{V}_{hcom}$ are the displacement volumes of the LCOM and HCOM of the heat pump obtained using the compressor's volumetric efficiency (Equation 7) and suction line volumetric flow rates. The temperature lift ($\Delta\bar{T}_{Lift}$) is calculated as the difference between the entropic average temperatures of the secondary fluids of the heat sink and source since they have considerable temperature gliding (i.e., $\Delta\bar{T}_{Lift} = \bar{T}_{hw} - \bar{T}_{cf}$). The DL-CRHP input modeling parameters at cycle design conditions and their variation ranges for heat sink (hot water) and heat source (chilled fluid) outlet temperature ranges are listed in Table 1.

Table 1. Input modeling parameters for performance simulation of the proposed DL-CRHP (shown in Figure 1).

Parameter and unit	Value (variation range)
Operating condition	
Chilled fluid supply temperature, t_{22} (°C)	−10 – +10
Hot water supply temperature, t_{25} (°C)	100 – 150
Design variables	
Absorber and evaporator minimum temperature difference, $\Delta T_{min,u}$ (°C)	5 and 3
Absorber cold end terminal temperature difference, $\Delta T_{abs,c}$ (°C)	15
Ammonia mass fraction at rectifier exit, z_{15} (kg/kg)	0.998
Cooler and RHX effectiveness, ε_{col} and ε_{rhx} (%)	90
Hot water (heat sink) temperature glide, $t_{hw,glide}$ (K)	30
Chilled fluid (heat source) temperature glide, $t_{cf,glide}$ (K)	10
Refrigeration capacity, $\dot{Q}_{eva}$ (kW)	500
SHX effectiveness, ε_{shx} (%)	80
Temperature glide of evaporation process, $t_{19} - t_{18}$ (K)	5

4. SIMULATION RESULTS AND DISCUSSION

The heat pump thermodynamic performance is evaluated at several chilled fluid supply temperatures, from −10 °C to 10 °C in steps of 5 °C, and design conditions are given in Table 1. Its sensitivity to hot water outlet temperature variation in the range of 100 °C to 150 °C is also assessed. Besides, there are technological constraints considered in the simulation of the DL-CRHP: • the water content of the compressed vapor is restricted up to 5% ($z_5 \geq 0.95$) since it is detrimental to the R717 compressor (Jensen *et al.*, 2015); • sub-atmospheric operating conditions of the heat pump

are avoided (i.e., $P_{low} > 1.0$ bar) to eliminate entrainment of air in the system (Jensen *et al.*, 2015); and • the compressors discharge temperature is limited up to 190 °C (t_7 and $t_9 \leq$190 °C) based on the current R717 compressor development (Bamigbetan *et al.*, 2017). This is to guarantee the lubricating oil thermal stability and reduce the effect of thermal stress, e.g., on the discharge line and gasket materials. However, Jensen *et al.* (2015) suggested that the discharge temperature limit can be increased up to 250 °C by replacing the lubricant (from mineral oil to synthetic oil), and with minor adjustments to the gasket materials and discharge line to tolerate the high-temperature condition. The maximum compression ratio in a single compression stage is limited to 8 for the considered piston compressor.

Figure 3A and 3B show the HCOM discharge pressure and temperature as a function of the hot water outlet temperature at different chilled fluid outlet temperatures and the design input conditions provided in Table 1. In the analyzed operating conditions of the DL-CRHP, the ammonia mass fraction of the compressed vapor is above 0.95 as depicted in Figure 3C except for chilled fluid and hot water delivery temperatures of –10 °C and 150 °C (which is $z_{com} = 0.9494$). The corresponding heating capacity of the DL-CRHP is shown in Figure 4D. The heat pump's low pressure is in the range of 2.6 bar to 5.6 bar when the child fluid outlet temperature is between −10 °C and 10 °C considering the assumed 5 K gliding of the partial vaporization process (stream 18→19) in the evaporator. When the hot water outlet temperature increases from 100 °C to 150 °C, the LCOM discharge temperature (t_7, in Figure 1) increases in the range of 124–182 °C, 121–178 °C, 119–175 °C, 117–172 °C, and 115–169 °C at the chilled fluid outlet temperatures of −10 °C, −5 °C, 0 °C, 5 °C, and 10 °C, respectively. The HCOM discharge temperature (see Figure 3B) is below 250 °C at any considered operating conditions of the heat pump. The isentropic efficiency value of the compressors (LCOM and HCOM) was about 0.786 in all considered operating conditions.

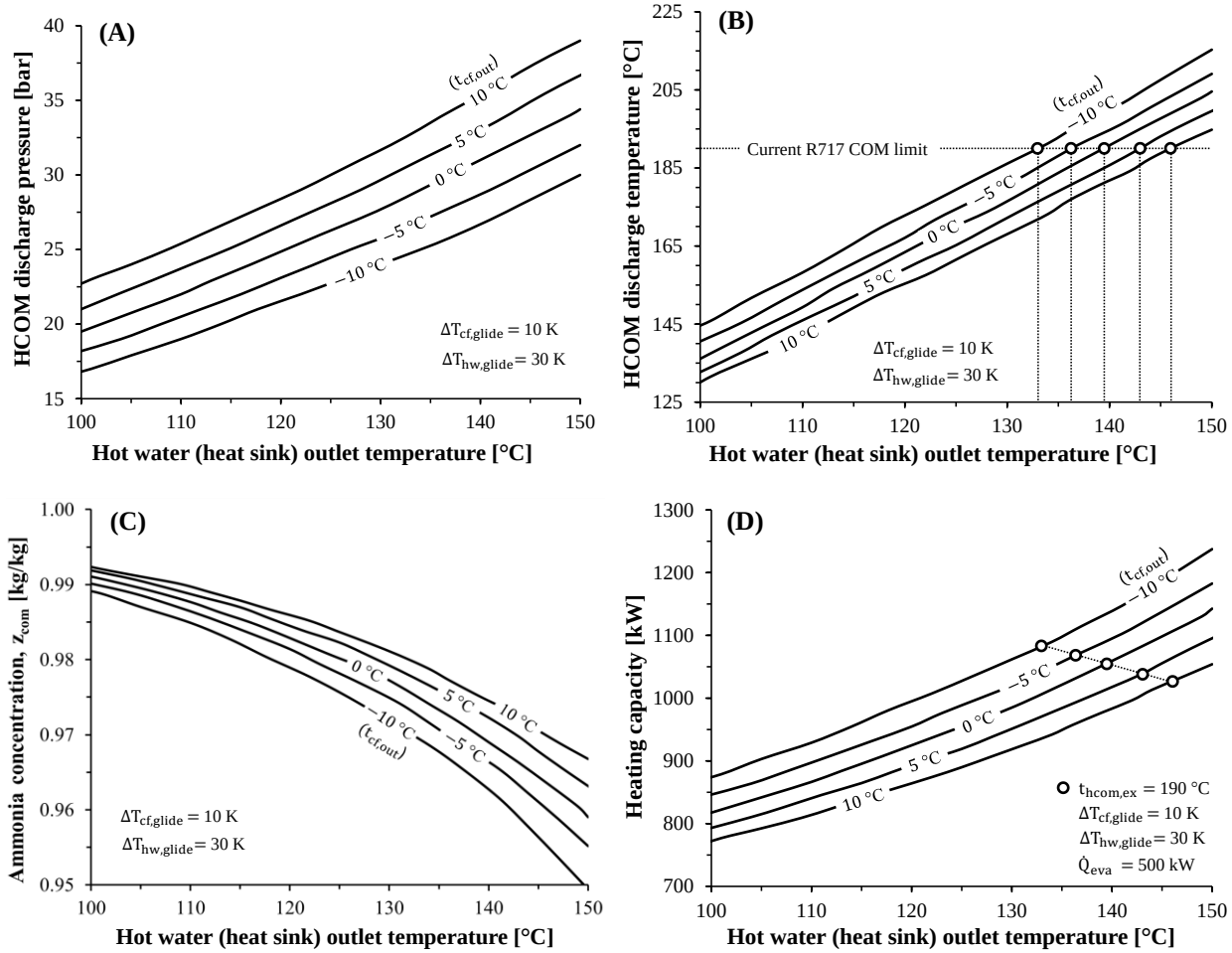

Figure 3: Effect of hot water (heat sink) outlet temperature on (A) high-stage compressor (HCOM) discharge pressure, (B) high-stage compressor (HCOM) discharge temperature, (C) compressed vapor ammonia concentration, and (D) heating capacity of the ammonia/water DL-CRHP.

When comparing the heating capacity of the DL-CRHP at different hot water supply temperatures and for a given chilled fluid supply temperature in Figure 3D, the heating capacity increases by about 41.8%, 38.6%, 39.2%, 37.6%, and 37.0% when the chilled fluid supply temperature is −10 °C, −5 °C, 0 °C, 5 °C, and 10 °C, respectively. This is due to the increases in the heat released by the absorber and desuperheating of the HCOM discharge in the gas cooler when the heat sink outlet temperature increases between 100 °C and 150 °C for all chilled fluid outlet temperatures considered, the absorber heat duty increased in the range of 756.7–999.7 kW, 740.0–964.6 kW, 719.7–939.0 kW, 703.1–909.7 kW, and 686.5–881.3 kW when chilled fluid outlet temperature is −10 °C, −5 °C, 0 °C, 5 °C, and 10 °C, respectively. The desuperheater (cooler) contributes approximately between 10.8% and 19.2% of the heating capacity of the heat pump when the heat sink outlet temperature increases between 100 °C and 150 °C.

The influence of hot water and chilled fluid outlet temperatures on the performance (i.e., COP_{shr}, $ECOP_{shr}$, and $\eta_{II,shr}$) and volumetric heating and refrigeration capacity (*VSHR*) of the DL-CRHP are evaluated in Figures 4A–4D. Other input modeling parameters are set according to their design values given in Table 1. The effect of hot water outlet temperature on the heat pump's combined COP (COP_{shr}) is shown in Figure 4A. When the hot water outlet temperature increased from 100 °C to 150 °C, the electrical power consumption of the heat pump ($\dot{W}_{lcom,el} + \dot{W}_{hcom,el} + \dot{W}_{sp,el}$) is also increased by about 97.8% (435.3–861.0 kW), 96.3% (405.9–796.7kW), 102.2% (370.9–750.0 kW), 103.6% (342.4–697.1 kW), and 105.5% (314.5–646.3 kW) when chilled fluid temperature is −10 °C, −5 °C, 0 °C, 5 °C and 10 °C, respectively. Thus, the combined effect of increased electricity consumption and heating capacity (Figure 4D) is a decrease in the combined COP of the DL-CRHP for any considered chilled fluid outlet temperature. The electrical power consumed to drive the solution pump is minor in contrast to the power consumption of the compressors, which is up to 2.1% of the heat pump's electrical power consumption.

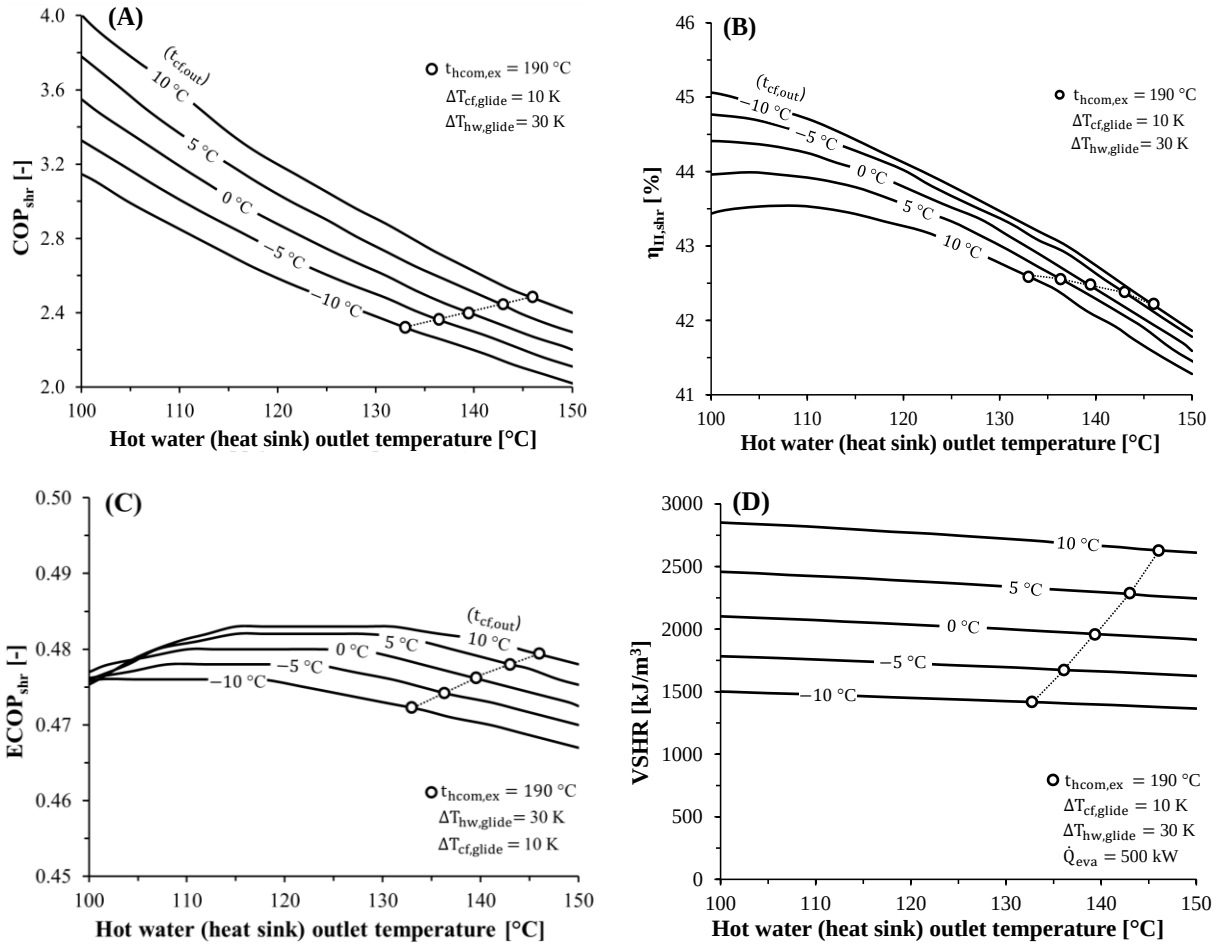

Figure 4: Effect of hot water (heat sink) outlet temperature on the performance of the proposed DL-CRHP. (A) combined COP (COP_{shr}), (B) second-law efficiency ($\eta_{II,shr}$), (C) exergy efficiency ($ECOP_{shr}$), and (D) *VSHR*.

Figure 4B illustrates the effect of the hot water outlet temperature on the second-law efficiency of the heat pump for simultaneous heating and refrigeration applications, $\eta_{II,shr}$, at the chilled fluid outlet temperatures of −10 °C to 10 °C. The ideal COP of the corresponding reversible heat pump, $COP_{ideal,shr}$, was decreased by about 31.1% (7.0–4.82), 31.9% (7.42–5.05), 34.9% (8.10–5.27), 35.6% (8.59–5.53), and 37.4% (9.30–5.82) when the hot water outlet temperature raised from 100 °C to 150 °C for the chilled fluid outlet temperatures of −10 °C, −5 °C, 0 °C, 5 °C, and 10 °C, respectively. In parallel, the combined COP values of the heat pump decrease, as shown in Figure 4A, as the hot water outlet temperature increases in the same range of chilled fluid outlet temperatures. Because of these combined effects, the second-law efficiency of the heat pump decreases from 45.1% to 43.3% when the hot water outlet temperature increases (100–150 °C). In the same considered operating range of the DL-CRHP, the temperature lift of the heat pump is between 90 K and 160 K when the lift is defined as the difference between the hot water and chilled fluid outlet temperatures, i.e., $\Delta T_{lift} = t_{hw,out} - t_{cf,out}$. While the mean temperature lift of the heat pump (i.e., $\Delta \bar{T}_{lift} = \bar{T}_{hw} - \bar{T}_{cf}$) becomes between 69 K and 140 K by considering the temperature gliding in the secondary fluids of the heat source and sink (10 K and 30 K, respectively). The concentration difference across the resorption solution circuit of the DL-CRHP ($\Delta z = z_s - z_w$) is between 0.14 and 0.16 in all operating ranges of the heat pump. With the standard R717 piston compressor technology constraints including the maximum allowed discharge pressure and temperature (i.e., 60 bar and 190 °C) and acceptable water (up to 5% in mass) in the compressed vapor, it is possible to reach a high heat (hot water) supply temperature of up to 133–146 °C using the DL-CRHP when the chilled fluid outlet temperature is between −10 °C and 10 °C.

The exergy efficiency of the DL-CRHP for simultaneous heating and refrigeration applications, $ECOP_{shr}$, is presented in Figure 4C. The exergy efficiency of the DL-CRHP varied marginally between 0.467 and 0.483 at the considered chilled fluid outlet temperatures (i.e., −10 °C to 10 °C) when the hot water outlet temperature increased from 100 °C to 150 °C. It is attributable due to the increased heat pump's heating capacity (see Figure 3D) and electrical power consumed by the heat pump, which are competing changes for the $ECOP_{shr}$ defined in Equation 14. Additionally, the Carnot factor used in Equation 14 (i.e., $1 - (T_0/\bar{T}_{hw})$) to account for the thermodynamic quality of the heating output of the heat pump is increased from 0.195 to 0.294 while both the refrigeration capacity and its corresponding Carnot factor was unchanged when the hot water outlet temperature varied from 100 °C to 150 °C. Figure 4D shows the influence of hot water and chilled fluid outlet temperatures on the VSHR of the DL-CRHP, which is decreased by approximately 9.2%, 8.6%, 8.8%, 8.6%, and 8.5% at the corresponding chilled fluid outlet temperature of −10 °C, −5 °C, 0 °C, 5 °C, and 10 °C, respectively, when the hot water outlet temperature increased 100–150 °C. The volumetric efficiency of both LCOM and HCOM, λ_{lcom} and λ_{hcom}, was decreased from 0.91 to 0.878, 0.916 to 0.886, 0.921 to 0.893, 0.926 to 0.9, and 0.93 to 0.906 as the hot water outlet temperature increased (100–150°C) when the chilled fluid outlet temperature is −10 °C, −5 °C, 0 °C, 5 °C, and 10 °C, respectively.

5. CONCLUSIONS

A double-lift ammonia/water compression-resorption heat pump (DL-CRHP) was proposed and thermodynamically evaluated for simultaneous process heating and refrigeration applications. The heat pump could meet the heating and refrigeration demands of various food and beverage processing industries. The heat pump cycle was designed for a hot water supply temperature of 100–150 °C with a heat sink gliding temperature of 30 K, while chilled fluid (ethylene glycol/water mixture) was provided simultaneously in the range of −10 °C and 10 °C at a heat source gliding temperature of 10 K for process cooling and storage applications. The combined heating and refrigeration COP of about 2.02–4.04 and exergy efficiency of about 0.47–0.48 was achievable with a heat sink outlet temperature of between 100 °C to 150 °C and refrigeration applications at a chilled fluid outlet temperature of −10 °C to 10 °C. The high-pressure compressor discharge temperature was reduced below the maximum allowed limit in the current R717 compressor technology ≤190 °C, in most of the analyzed operational conditions of the heat pump, by using the weak ammonia/water solution for the two-stage piston compressor intercooling. This allows hot water supply temperature of 133–146 °C when the refrigeration effect is provided at the temperature between −10 °C to 10 °C with the standard R717 compressor constraints (≤60 bar and ≤190 °C discharge pressure and temperature, and ≤5% water content is accepted in the compressed vapor).

In summary, the proposed DL-CRHP using ammonia/water mixture as a working fluid has several key features highly advantageous for its deployment to decarbonize the food and beverage processing industries including large-temperature-lift, heat sink temperature >100 °C, and design flexibility to adapt with the required heat sink and source temperature gliding for the heat pump integration.

NOMENCLATURE

COP	coefficient of performance (-)	t	temperature (°C)
CRHP	compression-resorption heat pump	VLHX	vapor liquid heat exchanger
DL	double-lift	VSHR	volumetric heat and refrigeration capacity (kJ m^{-3})
ECOP	exergy efficiency (-)	$\dot{W}$	electrical power (kW)
EG	ethylene glycol	z	ammonia mass fraction (kg kg^{-1})
HCOM	high-pressure stage compressor	ΔT	temperature difference/glide (K)
HX	heat exchanger	η_{II}	second-law efficiency (%)
LCOM	low-pressure stage compressor	**Subscript**	
$\dot{m}$	mass flow rate (kg s^{-1})	cf	chilled fluid
p	pressure (kPa or bar)	com	compressor
$\dot{Q}$	heat capacity/rate (kW)	hw	hot water
REV	refrigerant expansion valve	hcom	high-pressure compressor
RHX	refrigerant heat exchanger	lcom	low-pressure compressor
SEV	solution expansion valve	lift	temperature lift
SP	solution pump	shr	simultaneous heating and refrigeration

REFERENCES

Bamigbetan, O., Eikevik, T.M., Nekså, P., Bantle, M., 2017. Extending ammonia high temperature heat pump using butane in a cascade system, in: 7th IIR Conference: Ammonia and CO2 Refrigeration Technologies. IIF-IIR - France, Ohrid, North Macedonia, pp. 1–8. https://doi.org/10.18462/iir.nh3-co2.2017.0038

Erickson, D.C., Anand, G., Kyung, I., Makar, E., 2014. Heat-activated hot water heat pump and chiller, in: International Sorption Heat Pump Conference (ISHPC 2014), March 31-April 3. Washington DC, pp. 1–10.

Herold, K.E., Radermacher, R., Klein, S.A., 2016. Absorption chillers and heat pumps, Second. ed. CRC Press, Inc., Boca Raton.

IEA, 2014. Application of industrial heat pumps, Final report, Heat Pump Programme Annex 35/13.

Jensen, J.K., Markussen, W.B., Reinholdt, L., Elmegaard, B., 2015. On the development of high temperature ammonia-water hybrid absorption-compression heat pumps. Int. J. Refrig. 58, 79–89. https://doi.org/10.1016/j.ijrefrig.2015.06.006

Jørgensen, P.H., Ommen, T., Elmegaard, B., 2021. Quantification and comparison of COP improvement approaches for large-scale ammonia heat pump systems. Int. J. Refrig. 129, 301–316. https://doi.org/10.1016/j.ijrefrig.2021.04.016

Ladha-Sabur, A., Bakalis, S., Fryer, P.J., Lopez-Quiroga, E., 2019. Mapping energy consumption in food manufacturing. Trends Food Sci. Technol. 86, 270–280. https://doi.org/10.1016/j.tifs.2019.02.034

Liu, Y., Groll, E.A., Yazawa, K., Kurtulus, O., 2017. Energy-saving performance and economics of CO_2 and NH_3 heat pumps with simultaneous cooling and heating applications in food processing: Case studies. Int. J. Refrig. 73, 111–124. https://doi.org/10.1016/j.ijrefrig.2016.09.014

Meyers, S., Schmitt, B., Chester-Jones, M., Sturm, B., 2016. Energy efficiency, carbon emissions, and measures towards their improvement in the food and beverage sector for six European countries. Energy 104, 266–283. https://doi.org/10.1016/j.energy.2016.03.117

Ommen, T., Jensen, J.K., Meesenburg, W., Jørgensen, P.H., Pieper, H., Markussen, W.B., Elmegaard, B., 2019. Generalized COP estimation of heat pump processes for operation off the design point of equipment, in: 25th IIR International Congress of Refrigeration. Montreal, Canada, pp. 998–1005. https://doi.org/10.18462/iir.icr.2019.0648

Wersland, M.B., Eikevik, T., Tolstorebrov, I., 2018. Investigation of a hybrid compression absorption heat pump system for high temperatures, in: 13th IIR Gustav Lorentzen Conference. Valencia, Spain, pp. 815–822. https://doi.org/10.18462/iir.gl.2018.1283

Wersland, M.B., Kvalsvik, K.H., Bantlea, M., 2017. Off-design of high temperature hybrid heat pump, in: 12th IEA Heat Pump Conference. Rotterdam, the Netherlands, p. 12.

ACKNOWLEDGEMENT

The research work is funded by Diputació de Tarragona under the collaboration framework agreement between the Diputació de Tarragona and the Universitat Rovira i Virgili for the period 2020–2023